

neonSoilFlux: An R Package for Continuous Sensor-Based Estimation of Soil CO₂ Fluxes

John Zobitz¹ Edward Ayres² Zoey Werbin³ Ridwan Abdi¹
Natalie Ashburner-Wright⁴ Lillian Brown⁴
Ryan Frink-Sobierajski⁴ Lajntxiag Lee¹ Dijonë Mehmeti¹
Christina Tran⁴ Ly Xiong¹ Naupaka Zimmerman^{4,5}

¹ Augsburg University, 2211 Riverside Avenue, Minneapolis, MN 55454

² National Ecological Observatory Network, Battelle, 1685 38th Street, Suite 100, Boulder, CO 80301

³ Boston University, 5 Cummington Street, Boston, MA 02215

⁴ University of San Francisco, 2130 Fulton Street, San Francisco, CA 94117

⁵ University of Kansas, 1450 Jayhawk Boulevard, Lawrence, KS 66045

Acknowledgments

JZ acknowledges Kathleen O'Rourke for code development. NZ thanks technical staff at USF for support with field gear assembly and shipping. We thank the NEON field staff and assignable assets teams for facilitating each of the six NEON site visits. We are grateful

17 to LI-COR technical staff for helpful discussions about optimal soil chamber sampling methods.
18 This work was supported by NSF DEB grant #2017829 awarded to JZ, and NSF DEB grant
19 #2017860 awarded to NZ. This material is based in part upon work supported by the National
20 Ecological Observatory Network (NEON), a program sponsored by the U.S. National Science
21 Foundation (NSF) and operated under cooperative agreement by Battelle. We also thank the
22 reviewers and subject editor for their constructive feedback.

23 **Conflict of Interest Statements**

24 None of the authors have a financial, personal, or professional conflict of interest related to
25 this work.

26 **Author Contributions**

27 Conceptualization: JZ, NZ; Methodology: EA, JZ, NZ; Software: JZ, NZ, ZW, E A, DM, RA,
28 LX, LL; Validation: JZ, NZ; Formal Analysis: JZ, NZ, DM, RA, LX, LL; Investigation: JZ,
29 NZ, RF-S, CT, NA-W, LB; Resources: JZ, NZ; Data curation: JZ, NZ, DM, LX; Writing
30 – original draft: JZ, NZ; Writing – review and editing: JZ, NZ, ZW, EA, CT, DM, LX,;
31 Visualization: JZ, NZ, DM, RA, LX; Supervision: JZ; NZ; Project Administration: JZ; NZ;
32 Funding Acquisition: JZ; NZ

33 **Data Availability**

34 Anonymous field-collected data, `neonSoilFlux` calculated outputs, and manuscript-generating
35 code for peer review are provided as supplemental files. All will be made publicly available on

³⁶ Zenodo with a DOI upon publication.

1 Abstract

Accurate quantification of soil carbon fluxes is essential to reduce uncertainty in estimates of the terrestrial carbon sink. However, these fluxes vary over time and across ecosystem types and so it can be difficult to estimate them accurately across large scales. The flux gradient method estimates soil carbon fluxes using co-located measurements of soil CO₂ concentration, soil temperature, soil moisture, and other soil properties. The National Ecological Observatory Network (NEON) provides such data across 20 ecoclimatic domains spanning the continental U.S., Puerto Rico, Alaska, and Hawai'i. We present an R software package (`neonSoilFlux`) that acquires soil environmental data to compute half-hourly soil carbon fluxes for each soil replicate plot at a given terrestrial NEON site. To assess the computed fluxes, we visited six focal NEON sites and measured soil carbon fluxes using a closed-dynamic chamber approach. Outputs from the `neonSoilFlux` showed order-of-magnitude agreement to measured fluxes (R^2 between measured and `neonSoilFlux` outputs ranging from 0.00 to 0.78); measured outputs fell within the range of calculated uncertainties from the gradient method. Calculated fluxes from `neonSoilFlux` aggregated to the daily scale exhibited expected site-specific seasonal patterns. While the flux gradient method is broadly effective, its accuracy is highly sensitive to site-specific inputs, particularly estimates of soil diffusivity and moisture content. Future refinement and validation of `neonSoilFlux` outputs can contribute to existing databases of soil carbon flux measurements, providing near real-time estimates of a critical component of the terrestrial carbon cycle.

1.1 Keywords

Soil carbon, carbon dioxide, flux gradient, carbon cycle, field validation, soil respiration, ecosystem variability, diffusion

60 **2 Data for peer review**

61 Anonymous field-collected data, neonSoilFlux calculated outputs, and manuscript-generating
62 code for peer review are provided as supplemental files. All will be made publicly available on
63 Zenodo with a DOI upon publication.

64 **3 Introduction**

65 Soils contain the planet’s largest reservoir of terrestrial carbon (Jobbágy & Jackson, 2000). A
66 critical component of this reservoir is soil organic matter, the accumulation of which is influ-
67 enced by biotic factors such as above-ground plant inputs (Jackson et al., 2017). These inputs
68 in turn are influenced by environmental factors such as growing season length, temperature,
69 and moisture (Desai et al., 2022), which also affect the breakdown of soil organic matter and its
70 return to the atmosphere. Across heterogeneous terrestrial landscapes, the interplay between
71 these biotic and abiotic factors influence the size of the soil contribution to the terrestrial
72 carbon sink (Friedlingstein et al., 2025). However, the heterogeneity of these processes across
73 diverse ecosystems in the context of rapid environmental change leads to large uncertainty
74 about the magnitude of this sink in the future, and thus there remains a pressing need to
75 quantify changes in soil carbon pools and fluxes across scales.

76 Ecological observation networks such as the United States’ National Ecological Observatory
77 Network (NEON) and others (e.g. the globally-distributed FLUXNET or the European Inte-
78 grated Carbon Observation System) present a significant advancement in the nearly continuous
79 observation of biogeochemical processes at the continental scale. Notably, at 47 terrestrial sites
80 across the continental United States that span 20 ecoclimatic domains, NEON provides half-
81 hourly measurements of soil CO₂ concentration, temperature, and moisture at different vertical

82 depths. Each of these NEON sites also encompasses measurements of the cumulative sum of all
 83 ecosystem carbon fluxes in an airshed using the eddy covariance technique (Baldocchi, 2014).
 84 Soil observations provided by NEON are on the same timescale and standardized with eddy co-
 85 variance measurements from FLUXNET. These types of nearly continuous observational data
 86 (NEON and FLUXNET) can be used to reconcile differences between model-derived or data-
 87 estimated components of ecosystem carbon flux (Jian et al., 2022; Luo et al., 2011; Phillips et
 88 al., 2017; J. Shao et al., 2015; P. Shao et al., 2013; Sihi et al., 2016).

89 Estimated or observed soil carbon fluxes are a key metric for understanding change in soil
 90 carbon pools over time (Bond-Lamberty et al., 2024). A soil carbon flux to the atmosphere
 91 (F_S , units $\mu\text{mol m}^{-2} \text{s}^{-1}$), represents the aggregate process of transfer of soil CO_2 to the
 92 atmosphere from physical and biological processes (e.g. diffusion and respiration). Soil carbon
 93 fluxes can be assumed to encompass soil carbon respiration from autotrophic or heterotrophic
 94 sources (Davidson et al., 2006) and modeled with a exponential Q_{10} paradigm (Bond-Lamberty
 95 et al., 2004; Chen & Tian, 2005; Hamdi et al., 2013).

96 One common method by which F_S is measured in the field is through the use of soil chambers
 97 in a closed, well-mixed system (Norman et al., 1997) with headspace trace gas concentrations
 98 measured with an infrared gas analyzer (IRGA). F_S can also be estimated from soil CO_2
 99 measurements at different depths in the soil using the flux-gradient method (Maier & Schack-
 100 Kirchner, 2014). Closed-chamber IRGA measurements, while being the most common method,
 101 require either frequent in-person site visits or expensive and fragile automated systems. The
 102 potential of the gradient method is that fluxes can be estimated from continuous data recorded
 103 by robust solid-state sensors. The flux-gradient method is an approach that uses conservation
 104 of mass to calculate flux at a vertical soil depth z at steady state by applying Fick’s law of
 105 diffusion. A simplifying assumption for the flux-gradient method is that there is no mass trans-
 106 fer in the other spatial dimensions x and y (Maier & Schack-Kirchner, 2014). The diffusivity

107 profile, a key component of this calculation, varies across the soil depth as a function of soil
108 temperature, soil volumetric water content, atmospheric air pressure, and soil bulk density
109 (Millington & Shearer, 1971; Moldrup et al., 1999; Sallam et al., 1984).

110 Databases such as the Soil Respiration Database (SRDB) or the Continuous Soil Respiration
111 Database (COSORE) add to the growing network of resources for making collected observa-
112 tions of soil fluxes available to other researchers (Bond-Lamberty, 2018; Bond-Lamberty et
113 al., 2020; Bond-Lamberty & Thomson, 2010; Jian et al., 2021; Jiang et al., 2024). However,
114 these databases currently encompass primarily direct soil measurements of fluxes (i.e. those
115 using methods like the closed-chamber method described above). Currently, NEON provides
116 all measurements to calculate F_S from Fick’s law, but soil flux as a derived data product was
117 descoped from the initial network launch due to budget constraints (Berenbaum et al., 2015).
118 Deriving estimates of F_S using continuous sensor data across NEON sites thus remains a high
119 priority.

120 This study describes an R software package, `neonSoilFlux`, that computes a standardized
121 estimate of F_S at all terrestrial NEON sites using the flux-gradient method. Using direct
122 chamber-based field observations of soil carbon dioxide flux from a subset of terrestrial NEON
123 sites spanning six states, we provide a direct validation of F_S from `neonSoilFlux`.

124 Key objectives of this study are to:

- 125 1. Apply the flux-gradient method to estimate soil CO₂ flux from continuous sensor mea-
126 surements across six NEON sites.
- 127 2. Benchmark estimated soil carbon fluxes against field measurements (e.g. direct chamber
128 measurements of soil flux).
- 129 3. Identify sources of error in the flux-gradient approach across diverse sites in order to
130 guide future work.

131 **4 Materials and Methods**

132 **4.1 Field methods**

133 **4.1.1 Focal NEON Sites**

134 In order to acquire field data to validate model predictions of flux, we selected six terrestrial
135 NEON sites for analysis. We conducted roughly week-long field measurement campaigns at
136 these sites, which span a range of environmental gradients and terrestrial domains (Table 1).
137 SJER, SRER, and WREF were visited during May and June of 2022, and WOOD, KONZ,
138 and UNDE during May and June of 2024.

139 **4.1.2 Soil collar placement**

140 Either one (2022 sampling campaign) or two (2024 sampling campaign) PVC soil collars (20.1
141 cm inside diameter) were installed in close proximity to the permanent NEON soil sensors at
142 each site (Figure 1). As instruments in the NEON soil sensor arrays can occasionally break
143 down or stop working, the specific soil plot where we made measurements was chosen at each
144 site in consultation with NEON staff to maximize likelihood of quality soil sensor measurements
145 during the duration of the IRGA measurements. The plot selected at each site (out of the 5 in
146 each replicate array at each site) are presented in the last column of Table 1. After installation,
147 collar(s) were left to equilibrate for approximately 24 hours prior to any measurements being
148 taken.

4.1.3 Infrared gas analyzer measurements of soil CO₂ flux

In 2022, we then made measurements of flux on an hourly interval for 8 hours each day. Measurements were taken from roughly 8 am to 4 pm, with the time interval selected to capture the majority of the diurnal gradient of soil temperature each day. These measurements were made using a LI-6800 infrared gas analyzer instrument (LI-COR Environmental, Lincoln, NE) fitted with a soil chamber attachment (attachment 6800-09). In 2024, we again used the same LI-6800 instrument, but made half-hourly measurements over an approximately 8 hour period. In addition, in 2024 we also installed a second collar and used a second instrument, an LI-870 CO₂ IRGA, connected to an automated robotic chamber (LI-COR chamber 8200-104) controlled by an LI-8250 multiplexer to make automated measurements. The multiplexer was configured to take half-hourly measurements 24 hours a day for the duration of our sampling bout at each site. Each instrument was paired with a soil temperature and moisture probe (Stevens HydraProbe, Stevens Water, Portland, OR) that was used to make soil temperature and moisture measurements concurrent with the CO₂ flux measurements. Chamber volumes were set by measuring collar offsets at each site. System checks were conducted daily for the LI-6800 and weekly for the LI-8250. Instruments were factory calibrated before each field season.

Table 1: Listing of NEON sites studied for field work and analysis. Site refers to NEON site codes: Santa Rita Experimental Range (SRER), San Joaquin Experimental Range (SJER), Wind River Experimental Forest (WREF), Chase Lake National Wildlife Refuge (WOOD), Konza Prairie Biological Station (KONZ), and the University of Notre Dame Environmental Research Center (UNDE). Location is reported in decimal degrees of latitude and longitude. Other abbreviations include Mean Annual Temperature (MAT); $\overline{T_S}$: average soil temperature during field measurements; \overline{SWC} : average soil water content during field measurements. Dates refer to field measurement dates for each site. Plot refers to the particular location in the soil sensor array (denoted as HOR by NEON) where field measurements were made.

Site	Location	Ecosystem	MAT	$\overline{T_S}$	MAP	\overline{SWC}	Dates	Plot
SRER	31.91068, -110.83549	Shrubland	19.3 °C	47.6 °C	346 mm	4.0%	May 29– June 1 2022	004

Table 1: Listing of NEON sites studied for field work and analysis. Site refers to NEON site codes: Santa Rita Experimental Range (SRER), San Joaquin Experimental Range (SJER), Wind River Experimental Forest (WREF), Chase Lake National Wildlife Refuge (WOOD), Konza Prairie Biological Station (KONZ), and the University of Notre Dame Environmental Research Center (UNDE). Location is reported in decimal degrees of latitude and longitude. Other abbreviations include Mean Annual Temperature (MAT); $\overline{T_S}$: average soil temperature during field measurements; \overline{SWC} : average soil water content during field measurements. Dates refer to field measurement dates for each site. Plot refers to the particular location in the soil sensor array (denoted as HOR by NEON) where field measurements were made.

Site	Location	Ecosystem	MAT	$\overline{T_S}$	MAP	\overline{SWC}	Dates	Plot
SJER	37.10878,	Oak	16.4 °C	41.7 °C	540 mm	1.2%	June 1–4	005
	-119.73228	woodland					2022	
WREF	45.82049,	Evergreen	9.2 °C	15.3 °C	2225 mm	27.2%	June 7–9	001
	-121.95191	forest					2022	
WOOD	47.1282,	Restored	4.9 °C	14.9 °C	495 mm	14.9%	June 3–9	001
	-99.241334	prairie					2024	
KONZ	39.100774,	Tallgrass	12.4 °C	23.4 °C	870 mm	23.4%	May 29–	001
	-96.563075	prairie					June 1 2024	
UNDE	46.23391,	Deciduous	4.3 °C	13.0 °C	802 mm	13.0%	May 22–25	004
	-89.537254	forest					2024	

4.1.4 Post-collection processing of field data

We used LI-COR SoilFluxPro software (v 5.3.1) to assess the data after collection and to inform sampling parameters. We checked appropriateness of dead band and measurement durations using built-in evaluation tools. Based on this, the deadband period was set for 30-40 seconds, depending on the site, and the measurement duration was 180 seconds with a 30 second pre-purge and a 30 second post-purge at most sites, and a 90 sec pre- and post-purge at sites with higher humidity due to recent precipitation events. We also assessed the R^2 of linear and exponential model fits to measured CO_2 to verify measurement quality.

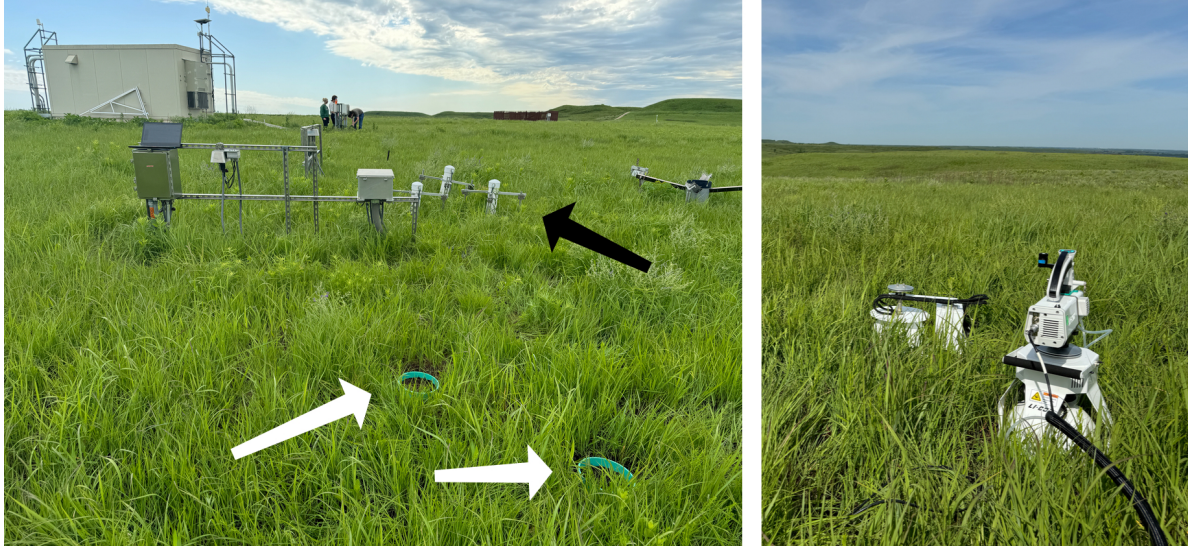


Figure 1: Spatial layout of field sampling using a closed-dynamic chamber setup at a representative NEON site (KONZ). Left image shows collars (white arrows) and permanent soil sensor installation (black arrow) and right image shows the LI-6800 (foreground) and LI-8200-104 (background) instruments placed on the collars.

4.2 neonSoilFlux R package

We developed an R package ([neonSoilFlux](#); Zobitz et al. (2024)) to compute half-hourly soil carbon fluxes and uncertainties from NEON data. The objective of the `neonSoilFlux` package is a unified workflow (Figure 2) for soil data acquisition and analysis that supplements the existing data acquisition R package (<https://CRAN.R-project.org/package=neonUtilities>; Lunch et al. (2025)).

At a given NEON site there are five replicate soil plots, each with measurements of soil CO₂ concentration, soil temperature, and soil moisture at different depths (Figure 3). The `neonSoilFlux` package acquires measured soil water content (National Ecological Observatory Network (NEON), 2024e), soil CO₂ concentration (National Ecological Observatory Network (NEON), 2024b), barometric pressure from the nearby tower (National Ecological Observatory Network (NEON), 2024a), soil temperature (National Ecological Observatory Network

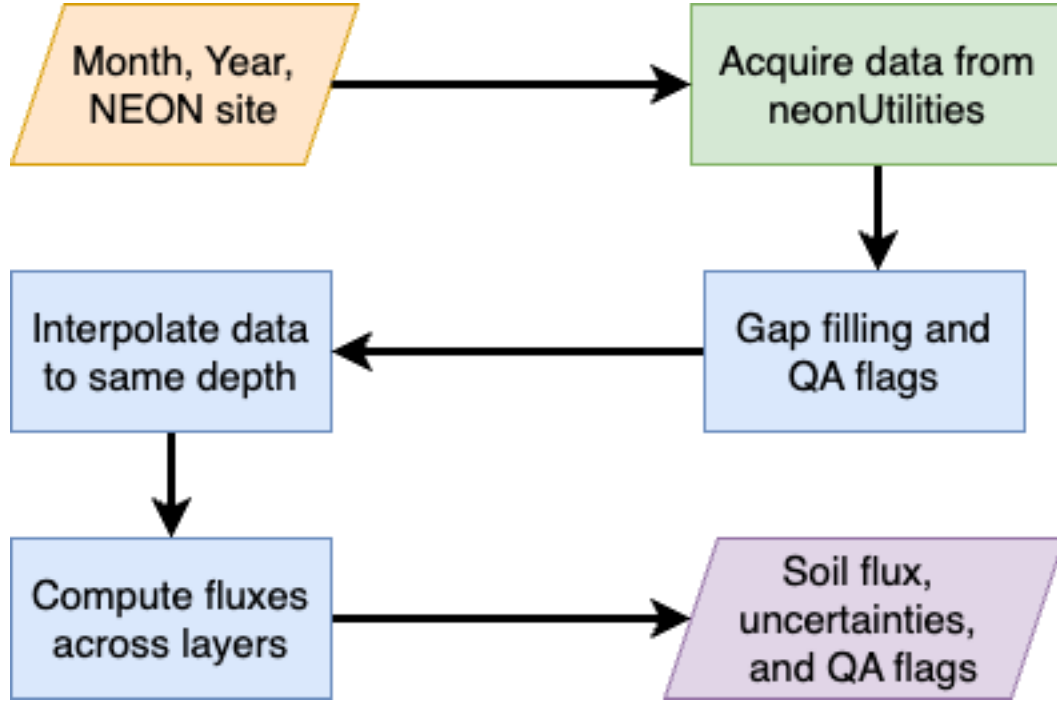


Figure 2: Diagram of `neonSoilFlux` R package. For a given month, year, and NEON site (orange parallelogram), the package acquires all relevant data to compute F_S using the `neonUtilities` R package (green rectangle). Data are gap-filled according to reported QA flags and interpolated to the same measurement depth before computing the soil flux, uncertainties, and final QA flags (blue rectangles). The package reports the associated soil flux, uncertainties, and quality assurance (QA) flags for the user (purple parallelogram).

186 (NEON), 2024d), and soil properties (e.g. bulk density) (National Ecological Observatory Net-
 187 work (NEON), 2024c). The static soil properties were collected from a nearby soil pit during
 188 site characterization and are assumed to be constant at each site. A soil flux calculation is
 189 computed at each replicate soil plot.

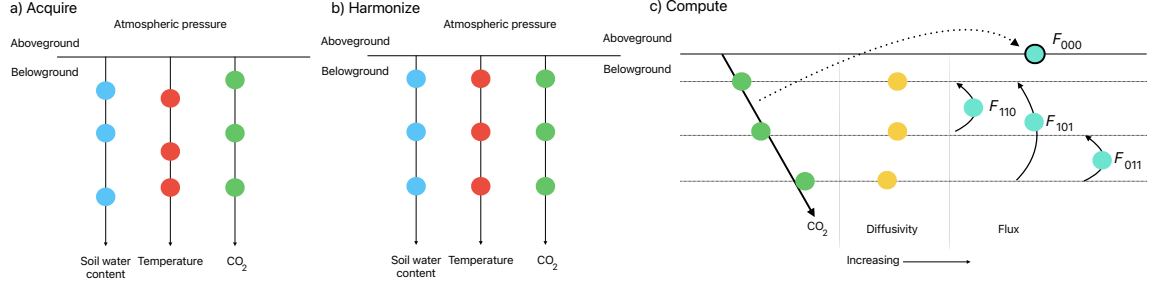


Figure 3: Model diagram for data workflow for the `neonSoilFlux` R package. a) Acquire: Data are obtained from given NEON location and horizontal sensor location, which includes soil water content, soil temperature, CO₂ concentration, and atmospheric pressure. All data are screened for quality assurance; if gap-filling of missing data occurs, it is flagged for the user. b) Any belowground data are then harmonized to the same depth as CO₂ concentrations using linear regression. c) The flux across a given depth is computed via Fick's law, denoted with F_{ijk} , where i, j , or k are either 0 or 1 denoting the layers the flux is computed across (i = closest to surface, k = deepest). F_{000} represents a flux estimate where the gradient dC/dz is the slope of a linear regression of CO₂ with depth.

190 The workflow to compute a value of F_S with `neonSoilFlux` consists of three primary steps,
 191 illustrated in Figure 3. First, NEON data are acquired for a given site and month via the
 192 `neonUtilities` R package (yellow parallelogram and green rectangle in Figure 2 and Panel
 193 a in Figure 3). Acquired environmental data can be exported to a comma separated value
 194 file for additional analysis. Quality assurance (QA) flags are reported as an indicator variable.
 195 Since the calibration coefficients on the soil water content sensors have changed over time
 196 (National Ecological Observatory Network (NEON), 2024e), raw sensor measurements were
 197 back-calculated and soil-specific calibrations were applied following Ayres et al. (2024) to
 198 generate a consistent time series at each measurement location.

199 The second step is harmonizing the data to compute soil fluxes across soil layers. This step
 200 consists of three different actions (blue rectangles in Figure 2 and Panel b in Figure 3). If a
 201 given observation by NEON is reported as not passing a quality assurance check, we applied
 202 a gap filling method to replace that measurement with its monthly mean at that same depth
 203 (Section 4.2.1). Belowground measurements of soil water and soil temperature are then inter-
 204 polated to the same depth as soil CO₂ measurements. The diffusivity (Section 4.2.2) and soil
 205 flux across different soil layers (Section 4.2.3) are then computed.

206 The third and final step is computing a surface soil flux through extrapolation to the sur-
 207 face (purple parallelogram in Figure 2 and Panel c in Figure 3). Uncertainty on a soil flux
 208 measurement is computed through quadrature. An aggregate quality assurance (QA) flag
 209 for each environmental measurement is also reported, representing if any gap-filled measure-
 210 ments were used in the computation of a soil flux. Within the soil flux-gradient method,
 211 several different approaches can be used to derive a surface flux (Maier & Schack-Kirchner,
 212 2014); the `neonSoilFlux` package reports four different possible values for soil surface flux
 213 (Section 4.2.3).

214 4.2.1 Gap-filling routine

215 NEON reports QA flags as binary values for each measurement and half-hourly interval. For
 216 a given half-hour, if any input variable (soil CO₂ concentration, soil temperature, or soil
 217 moisture) at depth z is flagged, computation of F_S is not possible. To address this, flagged
 218 measurements and their uncertainties were replaced with a bootstrapped monthly mean (\overline{m})
 219 and monthly standard deviation (\overline{s}) (Efron & Tibshirani, 1994).

220 For each month, depth z , and variable, we computed bootstrapped estimates of \overline{m} and \overline{s}
 221 from the vectors of unflagged measurements (\mathbf{m}), reported standard errors (σ), and the 95%

confidence interval (ϵ , or expanded uncertainty; Farrance & Frenkel (2012)). We also defined a bias vector $\mathbf{b} = \sqrt{\epsilon^2 - \sigma^2}$, which quantifies the spread of uncertainty in a given period and is incorporated into \overline{m} .

From these, 5000 bootstrap samples were generated for \mathbf{m}, σ , and \mathbf{b} . For each sample (m_k, b_k, σ_k) , we generated a vector \mathbf{n} (length $N = 5000$) by drawing from a normal distribution with mean $m_k + b_k$ and standard deviation σ_k . The sample mean and standard deviation were then computed from \mathbf{n} . The resulting distributions of sample means and sample standard deviations provided the bootstrapped monthly mean (\overline{m}) and standard error (\overline{s}) respectively.

This gap-filling procedure provides a consistent treatment across all data streams. However, alternative approaches may be better suited for longer gaps (e.g., correlations with other NEON measurement levels or soil plots) or for variable-specific conditions. We discuss the effect of gap-filling on our results in Section 6.1.

4.2.2 Soil diffusivity

Soil diffusivity D_a at a given measurement depth is the product of the diffusivity in free air $D_{a,0}$ ($\text{m}^2 \text{s}^{-1}$) and the tortuosity ξ (no units) (Millington & Shearer, 1971).

We compute $D_{a,0}$ with Equation 1:

$$D_{a,0} = 0.0000147 \cdot \left(\frac{T_i + 273.15}{293.15} \right)^{1.75} \cdot \left(\frac{P}{101.3} \right) \quad (1)$$

where T_i is soil temperature ($^{\circ}\text{C}$) at depth i (National Ecological Observatory Network (NEON), 2024d) and P surface barometric pressure (kPa) (National Ecological Observatory Network (NEON), 2024a).

Previous studies by Sallam et al. (1984) and Tang et al. (2003) demonstrated the sensitivity of modeled F_S depending on the tortuosity model (ξ) used to compute diffusivity. At low soil water content, the choice of tortuosity model can lead to order-of-magnitude differences in D_a , which in turn affect modeled F_S . The `neonSoilFlux` package currently includes two approaches to calculate ξ , representing the range of tortuosity behavior reported in Sallam et al. (1984).

The first approach is the Millington-Quirk model (Millington & Shearer, 1971), in which tortuosity depends on both porosity and soil water content:

$$\xi = \frac{(\phi - SWC_i)^{10/3}}{\phi^2} \quad (2)$$

In Equation 2, SWC is the soil water content at depth i (National Ecological Observatory Network (NEON), 2024e) and ϕ is the porosity, which in turn is a function of soil physical properties (National Ecological Observatory Network (NEON), 2024c):

$$\phi = \left(1 - \frac{\rho_s}{\rho_m}\right) (1 - f_V) \quad (3)$$

In Equation 3, ρ_m is the particle density of mineral soil (2.65 g cm^{-3}), ρ_s the soil bulk density (g cm^{-3}) excluding coarse fragments greater than 2 mm (National Ecological Observatory Network (NEON), 2024c), and f_V is a site-specific value that accounts for the proportion of soil fragments between 2-20 mm. Soil fragments greater than 20 mm were not estimated due to limitations in the amount of soil that can be analyzed (National Ecological Observatory Network (NEON), 2024c). We assume that rock fragments contain no internal pores.

The Millington-Quirk model assumes ξ is modulated by the amount of fluid saturation in soil pores (Millington & Shearer, 1971). In contrast, the Marshall model (Marshall, 1959)

expresses tortuosity as only a function of porosity ($\xi = \phi^{1.5}$), with ϕ defined from Equation 3. The Marshall model is independent of soil water content and assumes tortuosity is only governed by soil structure. The `neonSoilFlux` package allows users to choose the tortuosity model most appropriate for site-specific conditions and research goals.

4.2.3 Soil flux computation

We applied Fick's law (Equation 4) to compute the soil flux F_{ij} ($\mu\text{mol m}^{-2} \text{ s}^{-1}$) across two soil depths i and j :

$$F_{ij} = -D_a \frac{dC}{dz} \quad (4)$$

where D_a is the diffusivity ($\text{m}^2 \text{ s}^{-1}$) and $\frac{dC}{dz}$ is the gradient of CO_2 molar concentration ($\mu\text{mol m}^{-3}$, so the gradient has units of $\mu\text{mol m}^{-3} \text{ m}^{-1}$). The soil surface flux is theoretically defined by applying Equation 4 to measurements collected at the soil surface and directly below the surface. Measurements of soil temperature, soil water content, and soil CO_2 molar concentration across the soil profile allow for application of Equation 4 across different soil depths. Each site had three measurement layers, so we denote the flux as a three-digit subscript F_{ijk} with indicator variables i , j , and k indicate if a given layer was used (written in order of increasing depth), according to the following:

- F_{000} is a surface flux estimate using the intercept of the linear regression of D_a with depth and the slope from the linear regression of CO_2 with depth (which represents $\frac{dC}{dz}$ in Fick's Law). Tang et al. (2003) used this approach to compute fluxes in an oak-grass savannah.

- F_{110} , F_{011} are fluxes across the two most shallow layers and two deepest layers respectively. The diffusivity used in Fick’s Law is always at the deeper measurement layer. When used as a surface flux estimate we assume CO_2 remains constant above this flux depth.
- F_{101} is a surface flux estimate using linear extrapolation using concentration measurements between the shallowest and deepest measurement layer. Hirano et al. (2003) and Tang et al. (2005) used an approach similar to F_{101} in a temperate deciduous broadleaf forest and ponderosa pine forest respectively.

Uncertainty in all F_{ijk} is computed through quadrature (Taylor, 2022).

4.3 Post processing evaluation

Following collection of field measurements and calculation of the soil fluxes from `neonSoilFlux` package, we compared measured F_S based on closed-dynamic chamber measurements with the LI-COR instruments to a given soil flux calculation from `neonSoilFlux` for each site and flux computation method. Statistics included the , slope from a linear regression (m), normalized root mean squared error (NRMSE), and associated R^2 value.

Finally, for a half-hourly interval we also computed a *post hoc* D_a using the LI-COR flux along with the CO_2 surface gradient reported by NEON using the measurement levels closest to the surface.

Table 2: Summary of measured soil characteristics and flux results from field measurements across six NEON sites using a LI-COR 6800 (LI-870/8250 measurements omitted to enable direct comparability) via the closed-dynamic chamber method. Numeric values for soil CO₂ flux, soil temperature, and volumetric soil water content (VSWC) are the mean and standard deviation of field measurements at each site.

Site	Flux $\mu\text{mol m}^{-2} \text{ s}^{-1}$	Soil temp $^{\circ}\text{C}$	VSWC $\text{cm}^3 \text{ cm}^{-3}$	n
UNDE	2.55 ± 0.26	14.33 ± 0.77	0.33 ± 0.02	61
WOOD	3.02 ± 0.4	16.01 ± 1.54	0.28 ± 0.01	53
WREF	3.62 ± 0.3	15.34 ± 1.76	0.27 ± 0.06	21
KONZ	6.35 ± 0.97	27.28 ± 4.14	0.37 ± 0.01	44
SJER	0.94 ± 0.02	41.68 ± 11.22	0.01 ± 0.01	32
SRER	0.72 ± 0.09	47.64 ± 7.46	0.04 ± 0.01	32

5 Results

5.1 Concordance between modelled and measured soil CO₂ flux

The sites we visited ranged substantially in both their annual average temperature and precipitation as well as their biome type (Table 2). These differences also influenced the wide range of observed flux rates across sites.

The timeseries of the measured fluxes from the LI-COR 6800 and 870/8250 were compared to modeled soil fluxes from the `neonSoilFlux` R package (Figure 4). We also assessed year-long estimated flux time series and compared those to field measurements made at each site (Figure 5). Results are reported in local time. Where applicable, sites are displayed from left to right by increasing soil temperature (Table 1). Positive values of the flux indicate that there is a flux moving towards the surface. Overall, with the exception of SRER (discussed later) the computed fluxes determined using a variety of plausible methods spanned the field-measured fluxes, but the specific flux-gradient method that best approximated field measurements varied by site.

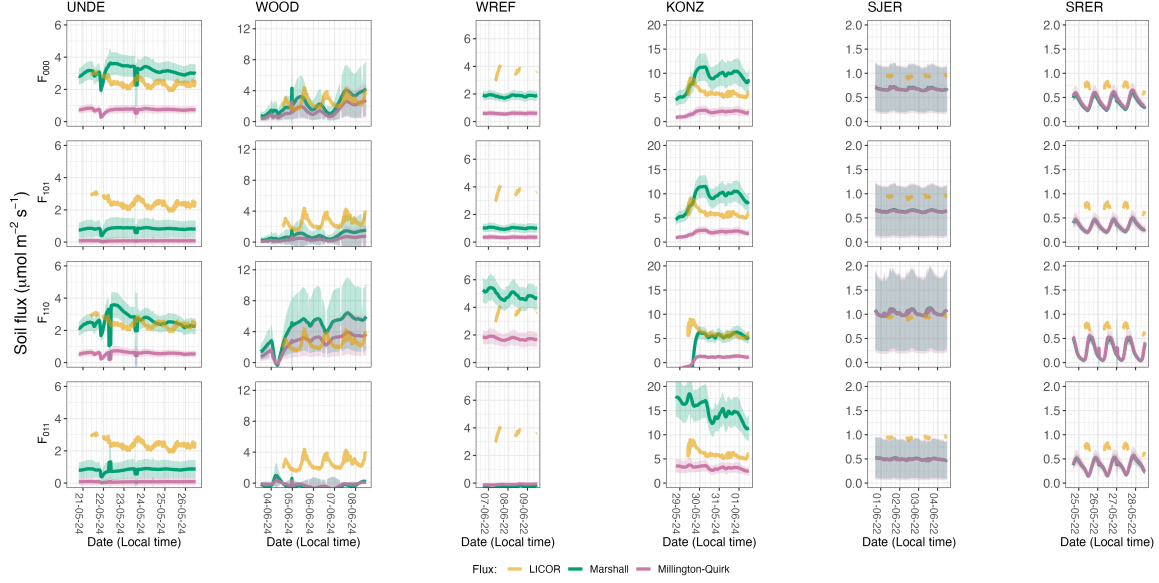


Figure 4: Timeseries of soil surface flux (F_S) from LICOR measured (yellow lines) and modeled soil fluxes (green or purple lines) by the `neonSoilFlux` R package. Fluxes from the `neonSoilFlux` R package are separated by the diffusivity model used (Millington-Quirk or Marshall, Section 4.2.2). Individual vertical axis labels in the first column represent the measurement levels where the flux-gradient approach is applied (Section 4.2.3). Ribbons for modeled soil fluxes represent ± 1 standard deviation. Results are reported in local time.

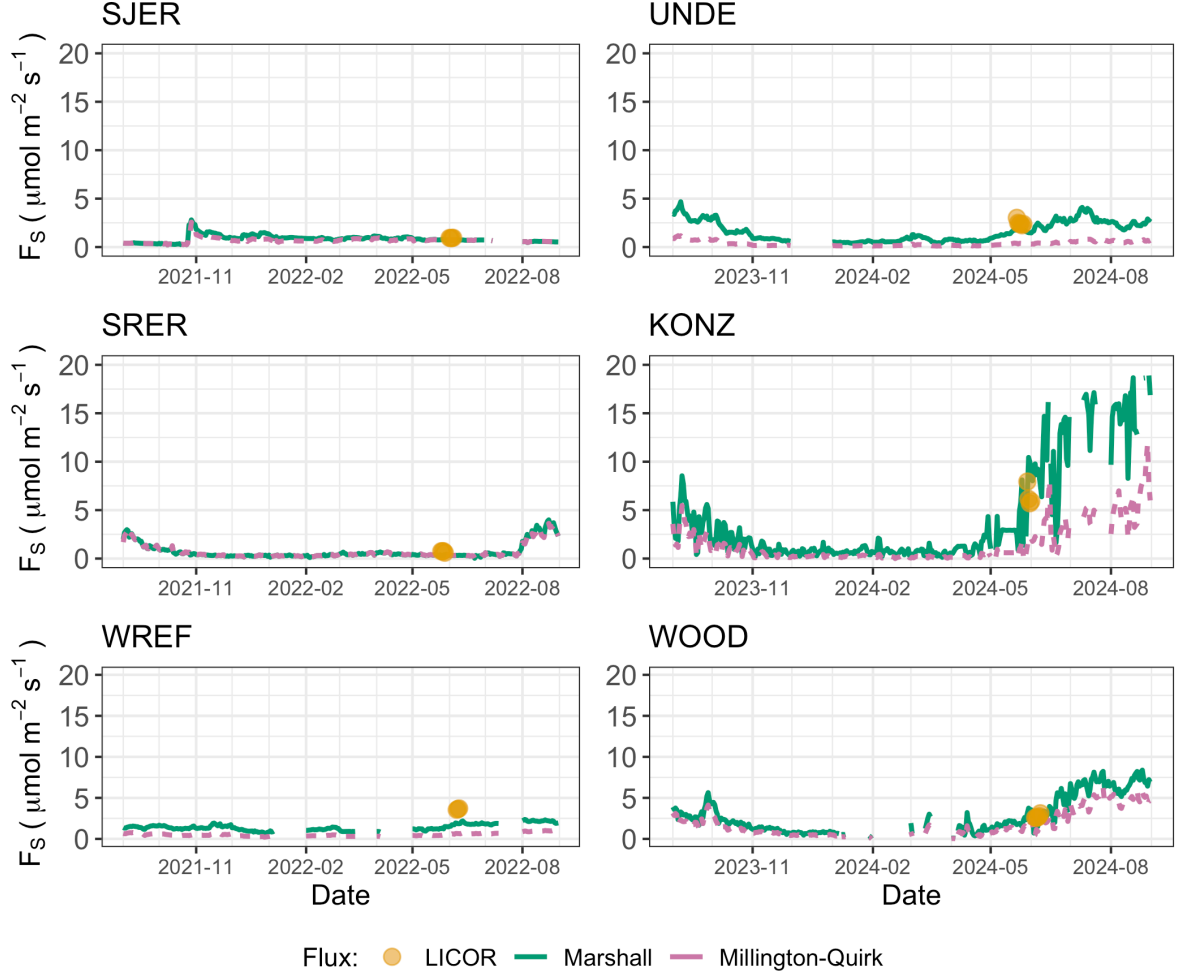


Figure 5: Timeseries of both daily-averaged field F_S (yellow circles) and daily ensemble averaged soil fluxes (average of F_{000} , F_{101} , F_{011} , F_{110} , Section 4.2.3) by the `neonSoilFlux` R package, separated by the diffusivity model used (green or purple lines, Millington-Quirk or Marshall, Section 4.2.2).

We calculated the statistical 1-1 comparison between the various estimates of soil flux computed by `neonSoilFlux` with the field-measured fluxes within half-hourly periods. Statistics for these comparisons are reported in Table 3.

5.2 Effects of method choice on diffusivity estimates

In four of six field sites, the *post hoc* D_a estimate fell roughly between the two diffusion estimation methods; however this was less the case in the two driest sites, SJER and SRER (Table 1), where the field estimate of diffusivity was either lower or higher than both of the other methods (Figure 6).

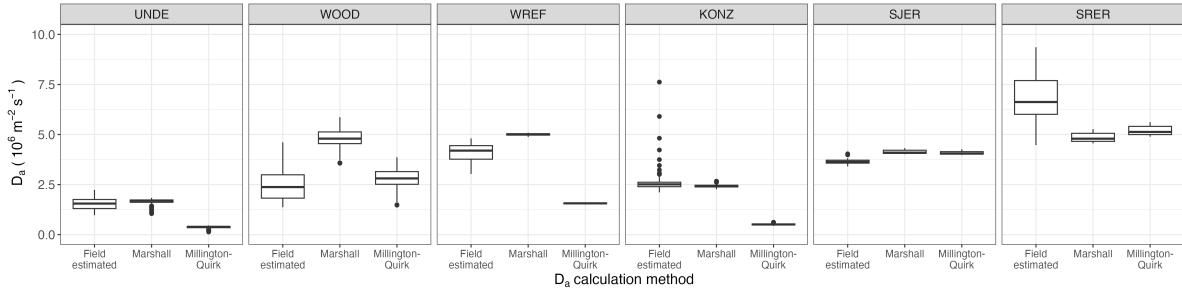


Figure 6: Distribution of diffusivity (D_a) at each study site. Values of D_a were provided by the `neonSoilFlux` package, computed from the Millington-Quirk or Marshall models (Section 4.2.2). A post-hoc estimate of diffusivity (labeled as “Field estimated”) was computed through the field measured flux (Figure 4), divided by the CO_2 gradient from the measurement levels closest to the soil surface, as reported by NEON. We only used F_S measured by the LICOR 6800 at all sites to standardize comparisons.

6 Discussion

This study presents a unified data science workflow to efficiently process automated measurements of belowground soil CO_2 concentrations, soil water content, and soil temperature to infer estimates of soil surface CO_2 effluxes through application of Fick’s Law (Equation 4).

Table 3: Statistical comparison between measured fluxes at each site with fluxes reported by `neonSoilFlux` with the different diffusivity calculations applied. m refers to the slope of a linear regression between the LICOR measured fluxes at each site and the outputs from `neonSoilFlux`. * = significance at the 5% level, ** = significance at the 1% level. NRMSE is the normalized root mean square error between measured and `neonSoilFlux` outputs, normalized by the sample mean of the LICOR measured fluxes.

	Millington-Quirk			Marshall		
	m	NRMSE	R^2	m	NRMSE	R^2
KONZ						
F_{110}	-0.39**	0.87	0.41	-1.86**	0.63	0.41
F_{101}	-0.12**	0.69	0.22	-0.44**	0.60	0.15
F_{011}	0.16**	0.52	0.20	1**	1.35	0.25
F_{000}	-0.12**	0.70	0.23	-0.41**	0.58	0.14
SJER						
F_{110}	-0.7*	0.13	0.17	-0.76*	0.14	0.18
F_{101}	-0.23*	0.32	0.21	-0.25**	0.31	0.24
F_{011}	-0.07	0.49	0.02	-0.09	0.48	0.03
F_{000}	-0.33*	0.29	0.17	-0.37*	0.28	0.18
SRER						
F_{110}	-0.06	0.56	0.00	-0.05	0.59	0.00
F_{101}	-0.34**	0.66	0.53	-0.33**	0.67	0.52
F_{011}	-0.44**	0.69	0.49	-0.42**	0.70	0.49
F_{000}	-0.48**	0.58	0.51	-0.44**	0.61	0.51
UNDE						
F_{110}	-0.09**	0.77	0.06	-0.29*	0.25	0.02
F_{101}	-0.01**	0.97	0.10	-0.1**	0.66	0.14
F_{011}	-0.01**	0.97	0.05	-0.09**	0.66	0.04
F_{000}	-0.11**	0.70	0.16	-0.29**	0.36	0.06
WOOD						
F_{110}	0.27**	0.31	0.10	0.32**	0.97	0.06
F_{101}	0.11**	0.87	0.16	0.19**	0.69	0.13
F_{011}	0.1**	1.12	0.10	0.23**	1.24	0.11
F_{000}	0.39**	0.47	0.16	0.55**	0.36	0.15
WREF						
F_{110}	-0.17**	0.53	0.78	-0.52**	0.35	0.75
F_{101}	-0.02*	0.91	0.24	-0.05**	0.73	0.35
F_{011}	0.05**	1.03	0.37	0.16**	1.07	0.37
F_{000}	0	0.84	0.00	-0.03	0.49	0.05

Our core goals in this study were: (1) to generate estimates of soil flux from continuous soil sensor data at terrestrial NEON sites using the flux-gradient method and then (2) to compare those estimates to field-measured fluxes based on the closed chamber approach at six NEON focal sites. We discuss our progress toward these core goals through (1) an overall evaluation of the flux-gradient approach (and uncertainty calculation) and (2) site-specific evaluation of differences in estimated vs measured fluxes.

6.1 General evaluation of flux-gradient approach

Key assumptions of the flux-gradient approach are that CO_2 concentrations increase throughout the soil profile such that the highest concentrations are observed in the deepest layers. Additionally, field flux measurements should correlate with F_{000} because they represent surface fluxes. Periods where this gradient condition are not met generally are connected to processes that occur during soil wetting events, where more shallow soil layers produce higher concentrations of CO_2 due to microbial respiration pulses following rewetting. This effect is likely to be largest at sites with rich organic soils (e.g. KONZ). Based on this reasoning, in these types of situations we would *a priori* expect F_{011} (deepest layers) $\leq F_{101} \leq F_{110}$ (shallow layers) $\leq F_{000}$ (all layers) because the previous flux estimates rely primarily on CO_2 concentrations at deeper depths, and could miss high concentrations of CO_2 produced in shallower layers.

When modeling soil respiration, typically a non-linear response function that also considers soil type is used (Bouma & Bryla, 2000; Yan et al., 2016, 2018). For the `neonSoilFlux` package, soil type is connected to the measurement of bulk density, which was characterized at each NEON site. This bulk density estimate is based on replicate samples collected from the site megapit at a subset of soil horizons, with an estimated uncertainty of $\pm 5\%$ (National Ecological Observatory Network (NEON), 2024c). Coarse fragment estimates also have very

large uncertainties, but because the volume fraction tends to be low in surface soils it probably wouldn't contribute much additional flux uncertainty.

Our results suggest that the most important way to improve reliability of the flux estimate is to reduce the usage of gap-filled data. The current approach to gap filling in `neonSoilFlux` uses monthly mean data to gap fill—this approach decreases the ability of the estimate to be responsive to short-term pulses that occur with rapid weather shifts. Four sites (KONZ, SRER, WREF, and UNDE) had more than 75% of half-hourly periods with no-gap filled measurements (Figure S1, Supplementary Information). Two sites (SJER and WOOD) had more than 75% of half-hourly intervals with just one gap-filled measurement. While we did not need to use gap-filled measurements to compute the flux at WREF, field data collection occurred following a severe rainstorm, with soils at the beginning of the sampling week near their water holding capacity. We recommend that whenever possible, knowledge of local field conditions should influence analysis decisions in addition to any QA filtering protocols in the `neonSoilFlux` package.

We recognize that this gap-filling approach may lead to gap-filled values that are quite different from the actual values, such as an underestimate of soil moisture following rain events. Further extensions of the gap filling method could use more sophisticated gap-filling routines, similar to what is used for net ecosystem carbon exchange (Falge et al., 2001; Liu et al., 2023; Mariethoz et al., 2015; Moffat et al., 2007; Zhang et al., 2023). The current gap-filling routine provides a consistent approach that can be applied to each data stream, but further work may explore alternative gap-filling approaches.

6.2 Evaluation of flux-gradient approach at each site

Derived results from the `neonSoilFlux` package have patterns that are broadly consistent with those directly measured in the field (Figure 4 and Figure 5), even though statistical comparisons between the field-measured and `neonSoilFlux` values were quite variable and poor (e.g. R^2 ranging from 0.00 to 0.78; Table 3). One advantage of the `neonSoilFlux` package is its ability to calculate fluxes across different soil depths (Figure 3), which allows for additional site-specific customization. We believe the package can provide a useful baseline estimate of soil fluxes that can always be complemented through additional field measurements.

The six locations studied provide a range of case studies that suggest different considerations may apply to different sites when applying the flux-gradient method. For example, the Santa Rita Experimental Range (SRER) is a desert site characterized by sandy soil, which also was the location of the highest field soil temperatures that we observed (Table 2). At SRER the flux across the top two layers (F_{110}) produced a pattern of soil flux most consistent with the observed field data. The remaining methods F_{101} , F_{011} , or F_{000} are derived from information taken from the deepest layer, which seems to have been decoupled from the surface layers both in terms of temperature and CO_2 concentration. This may be a general circumstance where there are large diurnal temperature extremes that rapidly change during the course of a day and overnight, leading to lags in the timing of when temperature increases propagate down to deeper soil layers.

Immediately prior to our visit to Konza Prairie (KONZ), that site that experienced a significant rain event that led to wet soils that gradually dried out over the course of our time there. This pulse of precipitation increased the soil CO_2 concentration at the top layer above the concentrations in lower layers, leading to negative estimated flux values at the start of the experiment. In this case it was only when the soil began to return to a baseline level that the assumptions of the flux-gradient method were again met.

Both of the previous cases also provide context for the poor statistical comparisons between field-measured soil fluxes and `neonSoilFlux` outputs Table 3. When considering systematic deployment of this method across a measurement network, there are a number of independent challenges that require careful consideration. There are clear tradeoffs between (1) accuracy of modeled fluxes (defined here as closeness to field-measured F_S and the uncertainty reduction factor ϵ), (2) precision (which could be defined by the signal to noise ratio), and (3) the choice of the diffusivity model (Section 4.2.2) or flux computation method (Section 4.2.3). A sensitivity analysis (Figure S2, Supplemental Information) found that flux output uncertainty was dominated by measurement uncertainty (T_S , P , SWC , or CO_2) rather than the diffusivity method to compute soil flux. Notably, the F_{110} method was least sensitive to measurement uncertainty likely because it best aligns with surface chamber measurement assumptions.

Finally, comparing the effects of different diffusivity estimation methods on the match between modeled and measured fluxes (Figure 5) highlights the sensitivity of F_{ijk} to diffusivity. The comparison between diffusivity estimates compared to field estimated diffusivity (Figure 6) demonstrates that site parameters can dictate which measure of diffusivity is most likely to be accurate in a given environmental context. Site-specific differences are largely a reflection of differences in soil moisture across the sites (Table 1), as not all diffusivity estimation methods incorporate soil moisture equivalently. While we here have compared two approaches to calculate diffusivity (the Millington-Quirk and Marshall models), it may be valuable to evaluate other diffusivity models (e.g. the Moldrup model; Moldrup et al. (1999)) as well. Ultimately the choice of a particular diffusivity model could be determined based on knowledge of site-specific evaluations or a set of these models could be used to generate a model ensemble average as a means to trade precision for a more general approach.

6.3 Recommendations for future method development

The `neonSoilFlux` package provides several approaches to estimate soil flux using the gradient method. We believe these approaches enable the software to be used across a range of site-specific assumptions (Maier & Schack-Kirchner, 2014). We note, however, that this choice can have a determinative approach on the calculated values. Ensemble averaging approaches (Elshall et al., 2018; Raftery et al., 2005) may be one way to address this problem if the goal is to calculate fluxes using the same method at a diverse range of different sites. Two other ideas would be to apply machine learning algorithms (e.g. random forests) to generate a single flux estimate across diverse sites, or using co-located estimates of net ecosystem carbon exchange from eddy-flux towers to further constrain results or to assess soil flux results for plausibility (Phillips et al., 2017).

These challenges notwithstanding, the method used here and made available in the `neonSoilFlux` R package has the potential to produce nearly continuous estimates of flux across all terrestrial NEON sites. These estimates are a significant improvement on available approaches to constrain the portion of ecosystem respiration attributable to the soil. This, in turn, also aids in our ability to understand the soil contribution to the net ecosystem flux measured at these sites using the co-located eddy flux towers.

7 Conclusions

We used the R package `neonSoilFlux` to test its broader application in estimating soil CO₂ fluxes with the flux-gradient method, using data from continuous buried soil sensors at NEON terrestrial sites. We compared the predicted fluxes to those measured directly using a field-based closed chamber approach. Soil fluxes from `neonSoilFlux` were broadly effective at producing estimates of flux comparable to those measured in the field using a chamber-based

technique. However **neonSoilFlux** outputs are quite sensitive to a number of issues, including: missing data (and thus gap-filling of input measurement datasets), the selection of soil depths used to best calculate the gradient (which may vary between sites), and finally the choice of method used for estimating soil diffusivity. The flexibility of the **neonSoilFlux** package allows the user to evaluate each of these issues with site-specific knowledge and contexts. Future refinements and subsequent validation of **neonSoilFlux** outputs will feed forward into evaluating soil carbon fluxes broader spatial scales to enhance understanding of the ways in which soils across diverse ecosystems are responding to a changing climate.

Sources Cited

- Ayres, E., Reichle, R. H., Colliander, A., Cosh, M. H., & Smith, L. (2024). Validation of Remotely Sensed and Modeled Soil Moisture at Forested and Unforested NEON Sites. *IEEE Journal of Selected Topics in Applied Earth Observations and Remote Sensing*, 17, 14248–14264. <https://doi.org/10.1109/JSTARS.2024.3430928>
- Baldocchi, D. (2014). Measuring fluxes of trace gases and energy between ecosystems and the atmosphere - the state and future of the eddy covariance method. *Global Change Biology*, 20(12), 3600–3609. <https://doi.org/10.1111/gcb.12649>
- Berenbaum, M. R., Carpenter, S. R., Hampton, S. E., Running, S. W., & Stanzione, D. C. (2015). *Report from the NSF BIO Advisory Committee Subcommittee on NEON Scope Impacts*.
- Bond-Lamberty, B. (2018). New Techniques and Data for Understanding the Global Soil Respiration Flux. *Earth's Future*, 6(9), 1176–1180. <https://doi.org/10.1029/2018EF000866>
- Bond-Lamberty, B., Ballantyne, A., Berryman, E., Fluet-Chouinard, E., Jian, J., Morris, K. A., Rey, A., & Vargas, R. (2024). Twenty Years of Progress, Challenges, and Opportunities in Measuring and Understanding Soil Respiration. *Journal of Geophysical Research:*

463 *Biogeosciences*, 129(2), e2023JG007637. <https://doi.org/10.1029/2023JG007637>
 464 Bond-Lamberty, B., Christianson, D. S., Malhotra, A., Pennington, S. C., Sihi, D., AghaK-
 465 ouchak, A., Anjileli, H., Altaf Arain, M., Armesto, J. J., Ashraf, S., Ataka, M., Baldocchi,
 466 D., Andrew Black, T., Buchmann, N., Carbone, M. S., Chang, S.-C., Crill, P., Curtis, P.
 467 S., Davidson, E. A., ... Zou, J. (2020). COSORE: A community database for continuous
 468 soil respiration and other soil-atmosphere greenhouse gas flux data. *Global Change Biology*,
 469 26(12), 7268–7283. <https://doi.org/10.1111/gcb.15353>
 470 Bond-Lamberty, B., & Thomson, A. (2010). A global database of soil respiration data. *Bio-*
 471 *geosciences*, 7(6), 1915–1926. <https://doi.org/10.5194/bg-7-1915-2010>
 472 Bond-Lamberty, B., Wang, C., & Gower, S. T. (2004). A global relationship between the
 473 heterotrophic and autotrophic components of soil respiration? *Global Change Biology*,
 474 10(10), 1756–1766. <https://doi.org/10.1111/j.1365-2486.2004.00816.x>
 475 Bouma, T. J., & Bryla, D. R. (2000). On the assessment of root and soil respiration for soils
 476 of different textures: Interactions with soil moisture contents and soil CO₂ concentrations.
 477 *Plant and Soil*, 227(1), 215–221. <https://doi.org/10.1023/A:1026502414977>
 478 Chen, H., & Tian, H.-Q. (2005). Does a General Temperature-Dependent Q₁₀ Model of Soil
 479 Respiration Exist at Biome and Global Scale? *Journal of Integrative Plant Biology*, 47(11),
 480 1288–1302. <https://doi.org/10.1111/j.1744-7909.2005.00211.x>
 481 Davidson, E. A., Janssens, I. A., & Luo, Y. (2006). On the variability of respiration in
 482 terrestrial ecosystems: Moving beyond Q₁₀. *Global Change Biology*, 12, 154–164. <https://doi.org/10.1111/j.1365-2486.2005.01065.x>
 483 <https://doi.org/10.1111/j.1365-2486.2005.01065.x>
 484 Desai, A. R., Murphy, B. A., Wiesner, S., Thom, J., Butterworth, B. J., Koupaei-Abyazani, N.,
 485 Muttaqin, A., Paleri, S., Talib, A., Turner, J., Mineau, J., Merrelli, A., Stoy, P., & Davis,
 486 K. (2022). Drivers of Decadal Carbon Fluxes Across Temperate Ecosystems. *Journal of*
 487 *Geophysical Research: Biogeosciences*, 127(12), e2022JG007014. [https://doi.org/10.1029/](https://doi.org/10.1029/2022JG007014)
 488 [2022JG007014](https://doi.org/10.1029/2022JG007014)

- 489 Efron, B., & Tibshirani, R. J. (1994). *An Introduction to the Bootstrap*. Chapman and
490 Hall/CRC. <https://doi.org/10.1201/9780429246593>
- 491 Elshall, A. S., Ye, M., Pei, Y., Zhang, F., Niu, G.-Y., & Barron-Gafford, G. A. (2018). Relative
492 model score: A scoring rule for evaluating ensemble simulations with application to micro-
493 bial soil respiration modeling. *Stochastic Environmental Research and Risk Assessment*,
494 *32*(10), 2809–2819. <https://doi.org/10.1007/s00477-018-1592-3>
- 495 Falge, E., Baldocchi, D., Olson, R., Anthoni, P., Aubinet, M., Bernhofer, C., Burba, G.,
496 Ceulemans, R., Clement, R., Dolman, H., Granier, A., Gross, P., Grünwald, T., Hollinger,
497 D., Jensen, N.-O., Katul, G., Keronen, P., Kowalski, A., Lai, C. T., ... Wofsy, S. (2001).
498 Gap filling strategies for defensible annual sums of net ecosystem exchange. *Agricultural*
499 *and Forest Meteorology*, *107*(1), 43–69. [https://doi.org/10.1016/S0168-1923\(00\)00225-2](https://doi.org/10.1016/S0168-1923(00)00225-2)
- 500 Farrance, I., & Frenkel, R. (2012). **Uncertainty of Measurement: A Review of the Rules**
501 **for Calculating Uncertainty Components through Functional Relationships**. *The Clinical*
502 *Biochemist Reviews*, *33*(2), 49–75.
- 503 Friedlingstein, P., O’Sullivan, M., Jones, M. W., Andrew, R. M., Hauck, J., Landschützer,
504 P., Le Quéré, C., Li, H., Luijkx, I. T., Olsen, A., Peters, G. P., Peters, W., Pongratz,
505 J., Schwingshackl, C., Sitch, S., Canadell, J. G., Ciais, P., Jackson, R. B., Alin, S. R., ...
506 Zeng, J. (2025). Global Carbon Budget 2024. *Earth System Science Data*, *17*(3), 965–1039.
507 <https://doi.org/10.5194/essd-17-965-2025>
- 508 Hamdi, S., Moyano, F., Sall, S., Bernoux, M., & Chevallier, T. (2013). Synthesis analysis
509 of the temperature sensitivity of soil respiration from laboratory studies in relation to
510 incubation methods and soil conditions. *Soil Biology and Biochemistry*, *58*, 115–126. <https://doi.org/10.1016/j.soilbio.2012.11.012>
- 512 Hirano, T., Kim, H., & Tanaka, Y. (2003). Long-term half-hourly measurement of soil CO₂
513 concentration and soil respiration in a temperate deciduous forest. *Journal of Geophysical*
514 *Research: Atmospheres*, *108*(D20). <https://doi.org/10.1029/2003JD003766>

515 Jackson, R. B., Lajtha, K., Crow, S. E., Hugelius, G., Kramer, M. G., & Piñeiro, G. (2017).
 516 The Ecology of Soil Carbon: Pools, Vulnerabilities, and Biotic and Abiotic Controls.
 517 *Annual Review of Ecology, Evolution and Systematics*, 48(Volume 48, 2017), 419–445.
 518 <https://doi.org/10.1146/annurev-ecolsys-112414-054234>

519 Jian, J., Bailey, V., Dorheim, K., Konings, A. G., Hao, D., Shiklomanov, A. N., Snyder, A.,
 520 Steele, M., Teramoto, M., Vargas, R., & Bond-Lamberty, B. (2022). Historically incon-
 521 sistent productivity and respiration fluxes in the global terrestrial carbon cycle. *Nature*
 522 *Communications*, 13(1), 1733. <https://doi.org/10.1038/s41467-022-29391-5>

523 Jian, J., Vargas, R., Anderson-Teixeira, K., Stell, E., Herrmann, V., Horn, M., Kholod, N.,
 524 Manzon, J., Marchesi, R., Paredes, D., & Bond-Lamberty, B. (2021). A restructured and
 525 updated global soil respiration database (SRDB-V5). *Earth System Science Data*, 13(2),
 526 255–267. <https://doi.org/10.5194/essd-13-255-2021>

527 Jiang, J., Feng, L., Hu, J., Liu, H., Zhu, C., Chen, B., & Chen, T. (2024). Global soil
 528 respiration predictions with associated uncertainties from different spatio-temporal data
 529 subsets. *Ecological Informatics*, 82, 102777. <https://doi.org/10.1016/j.ecoinf.2024.102777>

530 Jobbágy, E. G., & Jackson, R. B. (2000). The Vertical Distribution of Soil Organic Carbon
 531 and its Relation to Climate and Vegetation. *Ecological Applications*, 10(2), 423–436. [https://doi.org/10.1890/1051-0761\(2000\)010%5B0423:TVDOSO%5D2.0.CO;2](https://doi.org/10.1890/1051-0761(2000)010%5B0423:TVDOSO%5D2.0.CO;2)

533 Liu, K., Li, X., Wang, S., & Zhang, H. (2023). A robust gap-filling approach for European
 534 Space Agency Climate Change Initiative (ESA CCI) soil moisture integrating satellite
 535 observations, model-driven knowledge, and spatiotemporal machine learning. *Hydrology*
 536 *and Earth System Sciences*, 27(2), 577–598. <https://doi.org/10.5194/hess-27-577-2023>

537 Lunch, C., Laney, C., Mietkiewicz, N., Sokol, E., Cawley, K., & NEON (National Ecological
 538 Observatory Network). (2025). *neonUtilities: Utilities for working with NEON data*. <https://doi.org/10.32614/CRAN.package.neonUtilities>

540 Luo, Y., Ogle, K., Tucker, C., Fei, S., Gao, C., LaDeau, S., Clark, J. S., & Schimel, D. S. (2011).

Ecological forecasting and data assimilation in a data-rich era. *Ecological Applications*,
21(5), 1429–1442. <https://doi.org/10.1890/09-1275.1>

Maier, M., & Schack-Kirchner, H. (2014). Using the gradient method to determine soil gas
flux: A review. *Agricultural and Forest Meteorology*, 192–193, 78–95. <https://doi.org/10.1016/j.agrformet.2014.03.006>

Mariethoz, G., Linde, N., Jougnot, D., & Rezaee, H. (2015). Feature-preserving interpolation
and filtering of environmental time series. *Environmental Modelling & Software*, 72, 71–76.
<https://doi.org/10.1016/j.envsoft.2015.07.001>

Marshall, T. J. (1959). The Diffusion of Gases Through Porous Media. *Journal of Soil Science*,
10(1), 79–82. <https://doi.org/10.1111/j.1365-2389.1959.tb00667.x>

Millington, R. J., & Shearer, R. C. (1971). Diffusion in aggregated porous media. *Soil Science*,
111(6), 372–378.

Moffat, A. M., Papale, D., Reichstein, M., Hollinger, D. Y., Richardson, A. D., Barr, A. G.,
Beckstein, C., Braswell, B. H., Churkina, G., Desai, A. R., Falge, E., Gove, J. H., Heimann,
M., Hui, D., Jarvis, A. J., Kattge, J., Noormets, A., & Stauch, V. J. (2007). Comprehensive
comparison of gap-filling techniques for eddy covariance net carbon fluxes. *Agricultural and
Forest Meteorology*, 147(3), 209–232. <https://doi.org/10.1016/j.agrformet.2007.08.011>

Moldrup, P., Olesen, T., Yamaguchi, T., Schjønning, P., & Rolston, D. E. (1999). Modeling
diffusion and reaction in soils: 9. The Buckingham-Burdine-Campbell equation for gas
diffusivity in undisturbed soil. *Soil Science*, 164(2), 75.

National Ecological Observatory Network (NEON). (2024a). *Barometric pressure*
(DP1.00004.001). National Ecological Observatory Network (NEON). [https://doi.10.48443/RT4V-KZ04](https://doi.org/10.48443/RT4V-KZ04)

National Ecological Observatory Network (NEON). (2024b). *Soil CO2 concentra-*
tion (DP1.00095.001). National Ecological Observatory Network (NEON). <https://doi.org/10.48443/E7GR-6G94>

567 National Ecological Observatory Network (NEON). (2024c). *Soil physical and chemical proper-*
568 *ties, Megapit (DP1.00096.001)*. National Ecological Observatory Network (NEON). <https://doi.org/10.48443/S6ND-Q840>
569

570 National Ecological Observatory Network (NEON). (2024d). *Soil temperature (DP1.00041.001)*.
571 National Ecological Observatory Network (NEON). <https://doi.org/10.48443/Q24X-PW21>

572 National Ecological Observatory Network (NEON). (2024e). *Soil water content and water*
573 *salinity (DP1.00094.001)*. National Ecological Observatory Network (NEON). <https://doi.org/10.48443/A8VY-Y813>
574

575 Norman, J. M., Kucharik, C. J., Gower, S. T., Baldocchi, D. D., Crill, P. M., Rayment, M.,
576 Savage, K., & Striegl, R. G. (1997). A comparison of six methods for measuring soil-
577 surface carbon dioxide fluxes. *Journal of Geophysical Research: Atmospheres*, 102(D24),
578 28771–28777. <https://doi.org/10.1029/97JD01440>

579 Phillips, C. L., Bond-Lamberty, B., Desai, A. R., Lavoie, M., Risk, D., Tang, J., Todd-Brown,
580 K., & Vargas, R. (2017). The value of soil respiration measurements for interpreting and
581 modeling terrestrial carbon cycling. *Plant and Soil*, 413(1), 1–25. <https://doi.org/10.1007/s11104-016-3084-x>
582

583 Raftery, A. E., Gneiting, T., Balabdaoui, F., & Polakowski, M. (2005). *Using Bayesian Model*
584 *Averaging to Calibrate Forecast Ensembles*. <https://doi.org/10.1175/MWR2906.1>

585 Sallam, A., Jury, W. A., & Letey, J. (1984). Measurement of Gas Diffusion Coefficient under
586 Relatively Low Air-filled Porosity. *Soil Science Society of America Journal*, 48(1), 3–6.
587 <https://doi.org/10.2136/sssaj1984.03615995004800010001x>

588 Shao, J., Zhou, X., Luo, Y., Li, B., Aurela, M., Billesbach, D., Blanken, P. D., Bracho, R.,
589 Chen, J., Fischer, M., Fu, Y., Gu, L., Han, S., He, Y., Kolb, T., Li, Y., Nagy, Z., Niu, S.,
590 Oechel, W. C., ... Zhang, J. (2015). Biotic and climatic controls on interannual variability
591 in carbon fluxes across terrestrial ecosystems. *Agricultural and Forest Meteorology*, 205,
592 11–22. <https://doi.org/10.1016/j.agrformet.2015.02.007>

- Shao, P., Zeng, X., Moore, D. J. P., & Zeng, X. (2013). Soil microbial respiration from observations and Earth System Models. *Environmental Research Letters*, 8(3), 034034. <https://doi.org/10.1088/1748-9326/8/3/034034>
- Sihi, D., Gerber, S., Inglett, P. W., & Inglett, K. S. (2016). Comparing models of microbial–substrate interactions and their response to warming. *Biogeosciences*, 13(6), 1733–1752. <https://doi.org/10.5194/bg-13-1733-2016>
- Tang, J., Baldocchi, D. D., Qi, Y., & Xu, L. (2003). Assessing soil CO₂ efflux using continuous measurements of CO₂ profiles in soils with small solid-state sensors. *Agricultural and Forest Meteorology*, 118(3), 207–220. [https://doi.org/10.1016/S0168-1923\(03\)00112-6](https://doi.org/10.1016/S0168-1923(03)00112-6)
- Tang, J., Misson, L., Gershenson, A., Cheng, W., & Goldstein, A. H. (2005). Continuous measurements of soil respiration with and without roots in a ponderosa pine plantation in the Sierra Nevada Mountains. *Agricultural and Forest Meteorology*, 132(3), 212–227. <https://doi.org/10.1016/j.agrformet.2005.07.011>
- Taylor, J. R. (2022). *An Introduction to Error Analysis: The Study of Uncertainties in Physical Measurements, Third Edition* (3rd ed.). University Science Press.
- Yan, Z., Bond-Lamberty, B., Todd-Brown, K. E., Bailey, V. L., Li, S., Liu, C., & Liu, C. (2018). A moisture function of soil heterotrophic respiration that incorporates microscale processes. *Nature Communications*, 9(1), 2562. <https://doi.org/10.1038/s41467-018-04971-6>
- Yan, Z., Liu, C., Todd-Brown, K. E., Liu, Y., Bond-Lamberty, B., & Bailey, V. L. (2016). Pore-scale investigation on the response of heterotrophic respiration to moisture conditions in heterogeneous soils. *Biogeochemistry*, 131(1), 121–134. <https://doi.org/10.1007/s10533-016-0270-0>
- Zhang, R., Kim, S., Kim, H., Fang, B., Sharma, A., & Lakshmi, V. (2023). Temporal Gap-Filling of 12-Hourly SMAP Soil Moisture Over the CONUS Using Water Balance Budgeting. *Water Resources Research*, 59(12), e2023WR034457. <https://doi.org/10.1029/2023WR034457>

619 Zobitz, J., Ayres, E., O'Rourke, K., Werbin, Z., Lee, L., Abdi, R., Mehmeti, D., & Xiong, L.
620 (2024). *neonSoilFlux: Compute Soil Carbon Fluxes for the National Ecological Observatory*
621 *Network Sites*. <https://doi.org/10.32614/CRAN.package.neonSoilFlux>